

## Simultaneous Photo Catalysis of SiC/Fe<sub>3</sub>O<sub>4</sub> Nano-particles and Photo-fermentation of *Rhodospseudomonas* sp. nov. Strain A7 for Enhancing Hydrogen Production under Visible Light Irradiation

Bingfeng Liu,<sup>1\*</sup> Yaru Jin,<sup>1</sup> Guojun Xie,<sup>1</sup> Zhijiang Wang,<sup>2\*</sup> Hanquan Wen,<sup>1</sup> Nanqi Ren<sup>1</sup> and Defeng Xing<sup>1\*</sup>

To improve hydrogen production of photo-fermentation, synthetic SiC/Fe<sub>3</sub>O<sub>4</sub> nanoparticles with photocatalytic ability were added into the culture system of *Rhodospseudomonas* sp. strain A7. Results indicated that the hydrogen production was remarkably enhanced with the addition of 100 mg/L SiC/Fe<sub>3</sub>O<sub>4</sub> nanoparticles. The maximum volume and yield of hydrogen achieved 2474 mL/L-culture and 3.02 mol/mol-acetate, respectively. It was worth noting that photocatalysis and photo-fermentation were first realized simultaneously for hydrogen production with the SiC/Fe<sub>3</sub>O<sub>4</sub> nanoparticles. The mechanism of enhancement for producing hydrogen was also investigated. The bacterial aggregation performance was improved by the added SiC/Fe<sub>3</sub>O<sub>4</sub> nanoparticles. The activity of nitrogenase could be promoted while the activity of uptake hydrogenase could be inhibited. Beyond that, electron transfer behavior had taken place between strain A7 and nanoparticles. The electron transfer rate of the hydrogen production system could be promoted and accelerated by photo-generated electrons from SiC/Fe<sub>3</sub>O<sub>4</sub> nanoparticles. Hence, the hydrogen production ability and conversion efficiency of substrate were enhanced. The photocatalytic combining photo-fermentation is promising way for hydrogen production.

**Keywords:** Photocatalysis; Nanoparticles; Photo-fermentation; Hydrogen production.

**Received** 25 August 2018, **Accepted** 16 October 2018

**DOI:** 10.30919/esee8c160

### 1. Introduction

At present, the shortage of energy is a crucial issue in the world. Searching for clean, new, renewable energy resources and energy material to satisfy increasing energy demand is the promising way for sustainable development in the world.<sup>1,2</sup> Hydrogen as a sustainable energy carrier is hopeful to replace traditional fossil fuels in the near future.<sup>3</sup> Hydrogen gas produced by conventional methods has a limitation on the resource shortage and environmental pollution, hence hydrogen production by using biomass and photocatalysis has gained more attention in the past few years.<sup>4</sup> Photo-fermentation is a promising process for bio-hydrogen production and has extensive range and relatively high conversion efficiency of substrate.<sup>5</sup> However, there are some critical bottleneck problems need to solve for photo-fermentative hydrogen production, for example, low yield of hydrogen production, low utilization efficiency of substrate and poor conversion efficiency of light energy. Photocatalysis can produce hydrogen from water using light energy and has been widely applied.<sup>6</sup> Among varied photocatalysts, nanoparticles have been extensively investigated and applied in photocatalytic area, especially environmental treatment and

hydrogen production fields.<sup>7</sup>

Photobiocatalysis is a bio-photolysis by combining photocatalytic process and photo-biological technologies to produce hydrogen gas from water or other solution.<sup>8</sup> This provided a new possible avenue for improving biohydrogen production and light energy conversion efficiency of photo-fermentative bacteria. Few works have successfully reported photocatalysis nanoparticles can improve hydrogen production of photo-fermentation.<sup>9-13</sup> However, in those studies the simultaneous hydrogen generation by photocatalysis and photo-fermentation has not yet realized effectively and it is still a challenge. And widely used TiO<sub>2</sub> photocatalyst was applied as photocatalysis nanoparticles for improving hydrogen production of photo-fermentative bacteria in above reports. However, there are two main disadvantages of TiO<sub>2</sub> photocatalyst: one is the recombination of photo-generated electron, which decreases the quantum efficiency of the overall reaction<sup>14</sup> and the other is its poor thermal stability,<sup>15</sup> which decreases the photocatalytic performance and the quantum efficiency. Hence, researchers have prepared some materials, such as SnO<sub>2</sub> nanorods,<sup>16</sup> WO<sub>3</sub> nanorods<sup>17</sup> and graphene oxide (GO)<sup>18</sup> growth on TiO<sub>2</sub> nanofibers by different treatment methods, which successfully improved photocatalytic efficiency of TiO<sub>2</sub>. Recently, Silicon carbide (SiC) has attracted increasing attention as a promising semiconductor photocatalyst for hydrogen evolution from water due to its high photocatalytic activity, high chemical stability, and strong thermostability.<sup>19</sup> Our previous study first reported the SiC photocatalytic nanoparticles could obviously promote the hydrogen production of photo-fermentation bacterium *Rhodospseudomonas* sp. nov. strain A7.<sup>9</sup> And hydrogen yield has been enhanced 18.6% compared with alone strain A7, which is higher than that of TiO<sub>2</sub> nanoparticles. However, SiC nanoparticles still did not present any

<sup>1</sup>State Key Laboratory of Urban Water Resource and Environment, School of Environment, Harbin Institute of Technology, P.O. Box 2614, 73 Huanghe Road, Harbin 150090, China

<sup>2</sup>School of Chemistry and Chemical Engineering, Harbin Institute of Technology, Harbin 150001, China

\*E-mail: lbf@hit.edu.cn; wangzhijiang@hit.edu.cn; dxing@aliyun.com

photocatalytic activity from water or solution to hydrogen under visible light. Researchers have been reported that the photocatalytic ability of modified nanoparticles could be improved from water to hydrogen. The Pt/SiC catalyst shows an enhanced photocatalytic activity for water splitting. Hydrogen production rate of the Pt/SiC catalyst is 88% higher than that of SiC nanowires without the decoration of Pt nanoparticle.<sup>19</sup> Surface modified SiC through the acid oxidation exhibits excellent photocatalytic hydrogen evolution performance under visible light irradiation over that of unmodified SiC.<sup>20</sup> The water-splitting performance of the hybrid SnO<sub>2</sub>/SiC photoelectrode was also significantly enhanced compared with the pristine SiC nanowire photoelectrode.<sup>21</sup>

Therefore, to further improve the hydrogen production ability of combined system of photocatalysis and photo-fermentation, the modified SiC nanoparticles (SiC/PAA and SiC/Fe<sub>3</sub>O<sub>4</sub>) were first used in photo-fermentative hydrogen system. It was concluded that hydrogen production by photo-fermentation was significantly enhanced by the addition of SiC/Fe<sub>3</sub>O<sub>4</sub> nanoparticles with photocatalytic ability under visible light. It was noted that photocatalysis and photo-fermentation were realized simultaneously for hydrogen production with SiC/Fe<sub>3</sub>O<sub>4</sub> nanoparticles. Importantly, the strengthening mechanism of combined system of photo-fermentation bacteria and photocatalytic nanoparticles was analyzed and discussed in detail from different perspectives.

## 2. Experimental section

### 2.1 Bacterium and medium

The hydrogen producer, *Rhodospseudomonas sp nov. A7*, was used in this study.<sup>22</sup> The culture medium for the cell growth and hydrogen production of strain A7 were described by a previous report.<sup>22</sup> Acetate of 50 mmol/L and glutamate of 10 mmol/L were used as the sole carbon and nitrogen source in the medium for hydrogen production, respectively. The initial pH of medium was adjusted to 7.0.

### 2.2 Culture and operation conditions

The experiment of hydrogen production in batch culture was carried out in sealed reactors of 100 mL with the medium of 60 mL in triplicate. The argon was filled into the top space of the reactors for keeping anaerobic conditions. The reactors containing medium were autoclaved at a temperature of 21 °C lasting 15 min. The strain A7 of 10% (V/V) in the mid-exponential growth phase was inoculated into the reactors. The operation conditions of reactors were controlled as following: stirred speed of 120 rpm, fixed temperature of 35±1 °C and the intensity of illumination of 150 W/m<sup>2</sup> on the outside surface of the reactors.

### 2.3 Preparation of nanoparticles

The preparation of SiC nanoparticles was according to the following formula: SiO<sub>2</sub> particles, Si powder and multi wall carbon nanotubes were mixed at the mole ratio of 1:1:4 and ground for 1 h in a corundum crucible. Obtained the mixture was set in a sintering furnace and temperature was controlled at 1500 °C. And argon as protective gas was used and a flow rate was 10 L/h. The temperature of products were lowered to about 25 °C and then products were heated to 700 °C in air for eight hours to take away residual carbon from obtained products.<sup>23</sup>

SiC/PAA nanoparticles were synthesized by using following

process: SiC suspension was prepared with deionized water and ultrasonic vibration for 0.5 h. In the preparation process of SiC, polyacrylic acid (PAA) dispersants were added by stirring at least 1 h to obtain uniform mixture of PAA and SiC. After that, the products were centrifuged, dewatered and washed several times using deionized water, and then dried under vacuum condition at 60 °C.

The methods for synthesizing SiC/Fe<sub>3</sub>O<sub>4</sub> nanoparticles used the description of previous report.<sup>24</sup> SiC nanoparticles of 100 mg were added in TREG solution of 25 mL in ultrasonic vibration process to gain a uniform suspension. The iron precursor Fe(acac)<sub>3</sub> was added into the suspension and the mixture became well-distributed through ultrasonic treatment for more than 0.5 h. The resulting solution was heated to 287 °C in nitrogen with a flow rate of 3 °C/min by vigorous stirring. After cooling to about 25 °C, ethyl acetate of 30 mL was used to dilute the above solution, and the obtained products were washed several times. Residual reagents were removed by using ethanol and separation of SiC/Fe<sub>3</sub>O<sub>4</sub> nanoparticles was by a magnet. The obtained products were dried under vacuum condition with a temperature of 60 °C.

### 2.4 Analytical methods

A gas chromatograph (GC 9790, Fuli Analysis Instrument Company, Zhejiang) with a thermal conductivity detector and a 2 m packed column with 80-100 stationary phase was used to determine hydrogen concentration. Carrier gas and their flow rate were nitrogen gas and 50 mL/min, respectively. The detection of acetate concentration, light intensity, the bacterial concentration (OD<sub>660nm</sub>) and the agglutination index (F%) used previous reported methods.<sup>9</sup>

The measure of nitrogenase activity adopted the acetylene reduction method.<sup>25</sup> Sample of 5 mL were collected from reactor and transferred into a sterilized anaerobic tube of 25 mL. The mixture in the anaerobic tube was filled with argon to keep anaerobic environment and sealed with rubber plugs. Then anaerobic tubes were vented to atmospheric pressure and injected with acetylene gas of 4 mL. Finally the anaerobic tubes were incubated at the same conditions of hydrogen production for 12 h. After that, 25% trichloroacetic acid solution of 0.5 mL was added into the mixture to terminate the acetylene reduction reaction. The content of ethylene produced in the headspace of anaerobic tubes was assayed by the same analytical method as hydrogen. Nitrogenase activity was assayed by the formation amount of ethylene for per milliliter sample per hour.

Uptake hydrogenase activity was assayed according to Goodman.<sup>26</sup> Sample of 5 mL were removed from reactor and transferred into a sterilized anaerobic tube of 25 mL. The argon was filled into anaerobic tube to maintain anaerobic environment and tube was sealed with rubber plugs. Then anaerobic tubes were vented to atmospheric pressure and injected with hydrogen gas of 1 mL and 200 mmol/L K<sub>3</sub>Fe(CN)<sub>6</sub> solution of 1 mL. Finally, the anaerobic tubes were wrapped by tinfoil and put in the same hydrogen production condition with dark condition for 12 h. Uptake hydrogenase activity was assayed by the consumption amount of hydrogen for per milliliter sample per hour.

### 2.5 Characterization methods

The microstructure images of the nanoparticles and bacteria were observed on a Quanta 200FEG scanning electron microscope (SEM). The ultraviolet-visible absorption spectra (UV-Vis) were measured using an ultraviolet-visible spectrometer (UV-2550, Shimadzu,

Japan) with the wide scanning wavelength range (190-850 nm). The fluorescence spectra were determined by a fluorescence spectrometer (FP-6500, JASCO, Japan) with an excitation wavelength of 250 nm and emission wavelength range of 220-650 nm. The Raman spectra of nanoparticles and bacteria were examined by a Raman spectrometer (HR800, JY, France) with an argon ion excitation wavelength of 458 nm and scanning wavenumber range of 100-2000  $\text{cm}^{-1}$ . The phase composition of the experimental samples was analyzed by the X-ray diffraction (XRD) patterns using a X-ray diffractometer (D8 ADVANCE, BRUKER, Germany) equipped with a Cu K Alpha ( $\lambda=1.5418\text{\AA}$ ) source and  $10^\circ$ - $90^\circ$  diffraction angles range. The surface elements and functional groups of the experimental samples were analyzed by the X-ray photoelectron spectroscopic (XPS) patterns using a X-ray spectrometer (ESCALAB 250Xi, Thermo Fisher Scientific, USA) equipped with a Al K Alpha source. The zeta potential of the experimental samples in aqueous phase was tested by a zeta potential meter (Nano-Z, MALVERN, England).

### 3. Results

Our previous work has found that SiC nanoparticles could improve producing hydrogen performance of photo-fermentation, but it did not exhibit any photocatalytic activity from water or medium to hydrogen in producing hydrogen system under incandescent lamps irradiation.<sup>9</sup> Some studies have demonstrated that after the modification of nanoparticles, photocatalytic ability from water to hydrogen could occur or be promoted.<sup>27,28,29</sup> To further improve photo-hydrogen production by photocatalytic nanoparticles, SiC nanoparticles were modified by two methods of the surface modification and semiconductor compound modification. As a result, SiC/PAA and SiC/ $\text{Fe}_3\text{O}_4$  nanoparticles were obtained, respectively. So, this work investigated the effects of two kinds of nanoparticles on photo-fermentative hydrogen production.

#### 3.1 Hydrogen production by combined photo-fermentation and modified nanoparticles

The hydrogen production by combining strain A7 and SiC/PAA nanoparticles with different concentrations (0, 100, 200, 300 and 400 mg/L) was investigated (Fig. 1). The results showed that produced hydrogen of alone bacteria without nanoparticles (the control) reached 1849 mL/L-culture. However, no hydrogen was produced when alone SiC/PAA nanoparticles without bacteria were added in the medium, this was similar to alone SiC nanoparticles (Table 1). Cumulative hydrogen volume increased with the increasing concentration of SiC/PAA nanoparticles from 0 to 200 mg/L. At 200 mg/L of SiC/PAA nanoparticles, the maximum volume (2295 mL/L-culture) of hydrogen was obtained, which is 24.1% higher than that of the control. The excessive concentration of SiC/PAA nanoparticles also inhibited the biomass and hydrogen generation of bacteria.

The influences of SiC/PAA nanoparticles on the content and yield of hydrogen, cell growth ( $\text{OD}_{660\text{nm}}$ ) and acetate utilization were observed in Fig. S1. In 7 days of photo-fermentation, obtained the individual maximum value was 84.7%, 2.84 mol/mol-acetate, 4.19 and 36.1 mmol/L at 200 mg/L of SiC/PAA nanoparticles, respectively. Results were slightly higher than that with SiC nanoparticles (Table 1). The effects on hydrogen production performance of strain A7 by SiC/PAA were similar to SiC nanoparticles. The reason was that the surface modification method mainly changed surface properties to improve the dispersibility of

SiC/PAA nanoparticles. When suitable concentration of SiC/PAA nanoparticles was used, the aggregation ability of bacteria could be improved and the biomass increased quickly. Excessive concentration had an unfavorable effect on bacterial cell growth and hydrogen production.

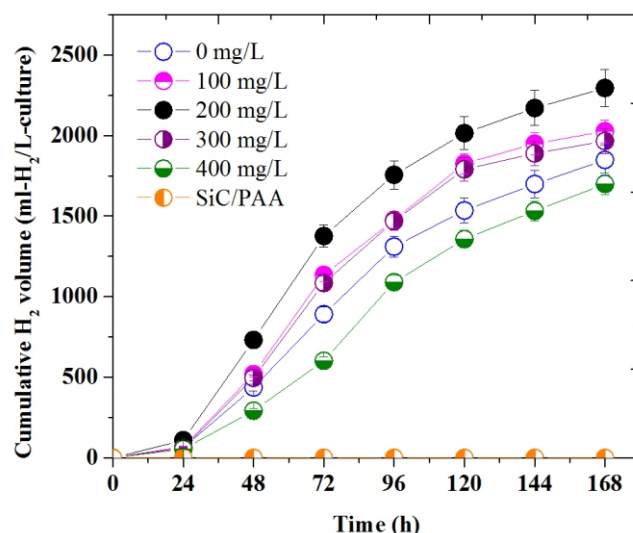


**Fig. 1** The influence of SiC/PAA nanoparticles of different concentration on the producing hydrogen by strain A7. (—○— the control, strain A7 without SiC/PAA nanoparticles —○— SiC/PAA nanoparticles of 100mg/L with strain A7 —●— SiC/PAA nanoparticles of 200mg/L with strain A7 —○— SiC/PAA nanoparticles of 300mg/L with strain A7 —●— SiC/PAA nanoparticles of 400mg/L with strain A7 —○— SiC/PAA nanoparticles without strain A7).

SiC/ $\text{Fe}_3\text{O}_4$  nanoparticles with different concentrations of 0-200 mg/L in photo-fermentative system obviously influenced on hydrogen evolution of strain A7 (Fig. 2). Alone strain A7 non-containing nanoparticles were used the control. The maximum cumulative hydrogen volume of the control reached 1841 mL/L-culture. Importantly, this work found that hydrogen gas of 4.21 mL/L-culture was generated when alone SiC/ $\text{Fe}_3\text{O}_4$  nanoparticles were putted in the photo-fermentation hydrogen production medium. This result was completely different from that with SiC and SiC/PAA nanoparticles. Photocatalytic decomposition of water or solution by SiC/ $\text{Fe}_3\text{O}_4$  nanoparticles took place in this experimental system. Simultaneous photocatalysis of SiC/ $\text{Fe}_3\text{O}_4$  nanoparticles and photo-fermentation of strain A7 for hydrogen production was realized successfully. The maximum cumulative hydrogen volume of 2474 mL /L-culture was obtained when the optimal concentration of SiC/ $\text{Fe}_3\text{O}_4$  nanoparticles was 100 mg/L. Compared to the control, hydrogen volume enhanced by 34.4%. The hydrogen yield was decreased gradually by the addition of excessive concentration (150 and 200 mg/L) of SiC/ $\text{Fe}_3\text{O}_4$  nanoparticles.

The effects of SiC/ $\text{Fe}_3\text{O}_4$  nanoparticles on average content of hydrogen, cell growth ( $\text{OD}_{660\text{nm}}$ ), acetate utilization and yield of hydrogen were investigated (Fig. S2). The maximal value of 88.9%, 4.22, 36.7 mmol/L and 3.02 mol- $\text{H}_2$ /mol-acetate was achieved at 100 mg/L SiC/ $\text{Fe}_3\text{O}_4$  nanoparticles, respectively. Those results were much higher than that with SiC and SiC/PAA nanoparticles. It was inferred that SiC/ $\text{Fe}_3\text{O}_4$  nanoparticles with photocatalysis ability generated photo-generated electrons and holes. Photo-generated electrons could produce hydrogen by using light energy and involve

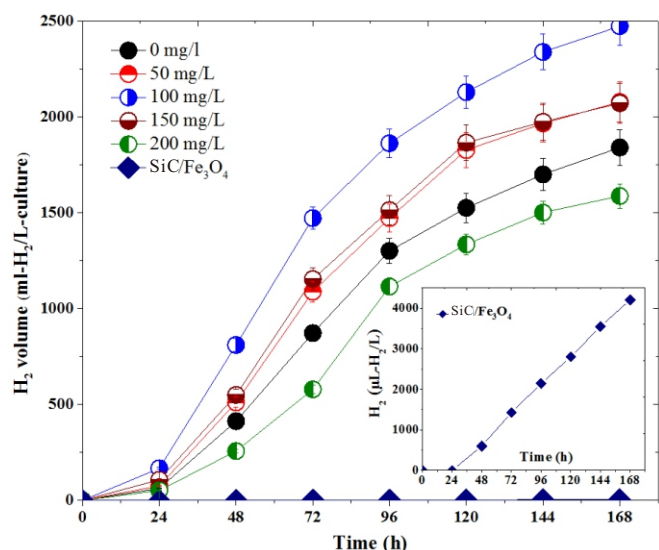


**Fig. 2** The effect of SiC/Fe<sub>3</sub>O<sub>4</sub> nanoparticles of different concentrations on hydrogen production by strain A7. (● the control, strain A7 without SiC/Fe<sub>3</sub>O<sub>4</sub> nanoparticles; ● SiC/Fe<sub>3</sub>O<sub>4</sub> nanoparticles of 50 mg/L with strain A7; ● SiC/Fe<sub>3</sub>O<sub>4</sub> nanoparticles of 100 mg/L with strain A7; ● SiC/Fe<sub>3</sub>O<sub>4</sub> nanoparticles of 150 mg/L with strain A7; ● SiC/Fe<sub>3</sub>O<sub>4</sub> nanoparticles of 200 mg/L with strain A7; ● SiC/Fe<sub>3</sub>O<sub>4</sub> nanoparticles without strain A7)

in the electron transfer system of photosynthetic bacteria. And photo-generated holes could participate in oxidation reactions with substances in the medium to produce oxidative radical (OH, O<sub>2</sub><sup>-</sup>) or substances (H<sub>2</sub>O<sub>2</sub>, O<sub>3</sub>) promoting the degrading of the substance utilized by strain A7. When SiC/Fe<sub>3</sub>O<sub>4</sub> nanoparticles were in the excessive concentration range, bacterial biomass decreased quickly. The reason may be due to low penetration of light and oxidative radical caused by SiC/Fe<sub>3</sub>O<sub>4</sub> nanoparticles, so bacterial metabolic activity was inhibited and biomass was in lower levels.

The comparison of effects of SiC and modified SiC nanoparticles on photo-fermentation hydrogen production showed in Table 1. The results clearly indicated that both of SiC and modified SiC nanoparticles can obviously improve the hydrogen production performance of the strain A7. The optimal concentration of SiC/PAA

and SiC/Fe<sub>3</sub>O<sub>4</sub> nanoparticles were 200 and 100 mg/L, respectively. SiC/Fe<sub>3</sub>O<sub>4</sub> nanoparticles were better than SiC and SiC/PAA because of the higher photocatalytic efficiency. The maximum cumulative volume, content and yield of hydrogen and biomass were achieved when SiC/Fe<sub>3</sub>O<sub>4</sub> nanoparticles existed in the photo-fermentation hydrogen production system. And the yield of hydrogen and biomass were increased by 34.4% and 26% compared to the controls, respectively. Thus, the capacity of producing hydrogen by photo-fermentation was significantly enhanced by the adding SiC/Fe<sub>3</sub>O<sub>4</sub> nanoparticles with photocatalytic ability in this study.

To further explain the reason for enhanced hydrogen evolution by photosynthetic bacterium strain A7 and SiC/Fe<sub>3</sub>O<sub>4</sub> nanoparticles with photocatalytic ability, this work explored following characterizations from nanoparticles and bacteria.

### 3.2 The characterizations of nanoparticles for enhancing H<sub>2</sub> production

The SEM images of nanoparticles were displayed in Fig. 3a-c. As seen from the microstructure of nanoparticles, SiC nanoparticles and SiC/PAA were rough and variable in size, SiC/Fe<sub>3</sub>O<sub>4</sub> nanoparticles showed round appearance and uniform distribution indicating that Fe<sub>3</sub>O<sub>4</sub> was successfully loaded on SiC nanoparticles and changed the surface topography of SiC nanoparticles.

The ultraviolet-visible absorption spectra (UV-Vis) of SiC, SiC/PAA and SiC/Fe<sub>3</sub>O<sub>4</sub> nanoparticles were presented in Fig. 4a. The spectra gave the information about the absorption of light in the wavelength range of 190-850 nm. SiC and SiC/PAA nanoparticles had similar absorption spectra because the surface modification method mainly changed surface properties to improve the dispersibility. And PAA coating on the surface of SiC reduced light utilization so that SiC/PAA nanoparticles had lower absorption of light. On the contrary, SiC/Fe<sub>3</sub>O<sub>4</sub> nanoparticles showed higher absorption values during wavelength range of 450-800 nm, which closed to absorption range of wavelength of photo-fermentation bacteria. This work found that visible light absorption range of synthetic SiC/Fe<sub>3</sub>O<sub>4</sub> nanoparticles by the semiconductor compound modification was significantly improved. This is direct reason that led to the increase of photocatalytic ability from water or medium to hydrogen and final yield of hydrogen evolution in combined system was increased.

To explore photocatalysis efficiency of modified nanoparticles,

**Table 1.** The comparison of effects of SiC and modified SiC nanoparticles on hydrogen evolution of strain A7.

Samples	H <sub>2</sub> volume mL/L-culture	H <sub>2</sub> content %	The maximum OD <sub>660nm</sub>	Acetate utilization mmol/L	H <sub>2</sub> yield mol/mol-acetate	End pH
Alone Strain A7	1846±38	82.1±1.0	3.35±0.2	31.2±0.5	2.65±0.1	7.48
Strain A7 with SiC	2230±23	84.1±0.6	4.18±0.1	35.3±0.4	2.82±0.1	7.54
Strain A7 with SiC/PAA	2295±25	84.7±0.4	4.19±0.1	36.2±0.3	2.84±0.1	7.45
Strain A7 with SiC/Fe <sub>3</sub> O <sub>4</sub>	2474±19	88.9±0.1	4.22±0.2	36.7±0.1	3.02±0.1	7.50

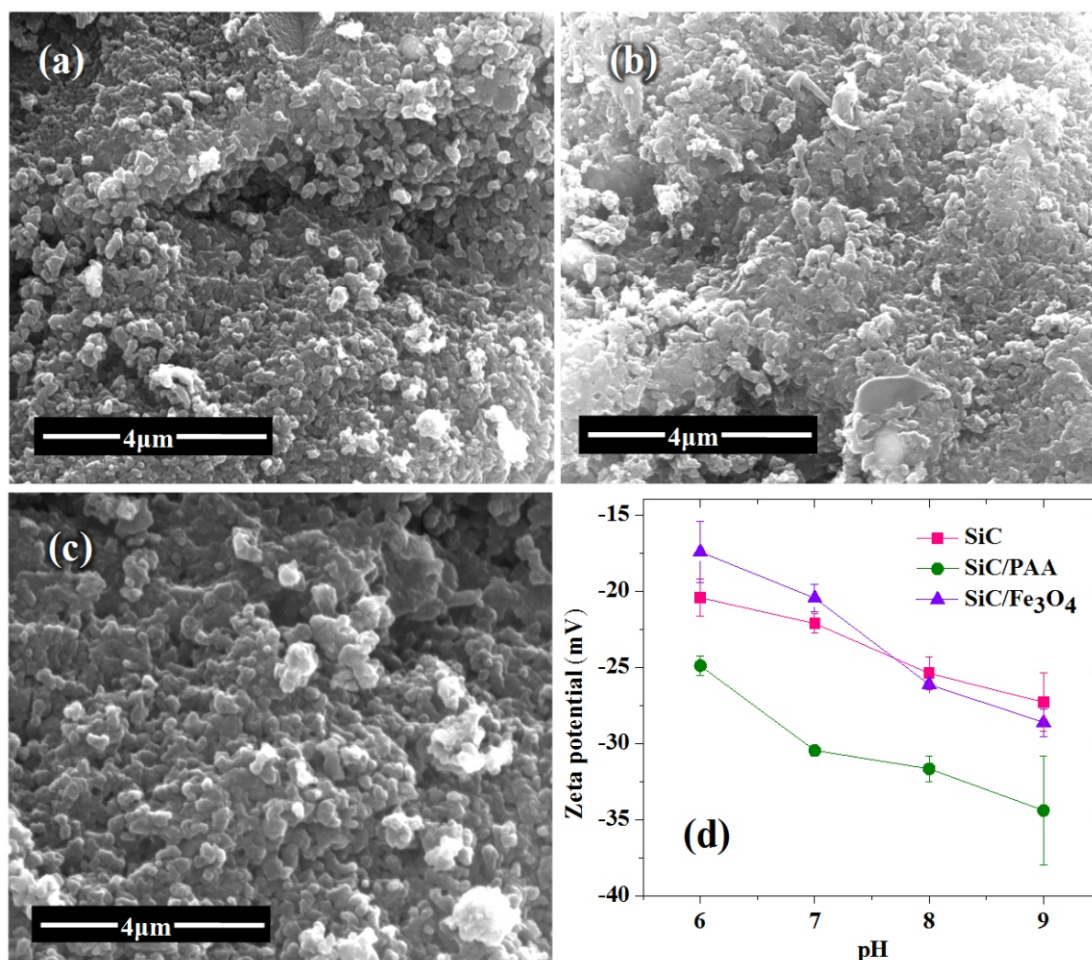


**Fig. 3** The SEM images and Zeta potential of nanoparticles. a) SiC. b) SiC/PAA. c) SiC/Fe<sub>3</sub>O<sub>4</sub>. d) Zeta potential of different nanoparticles.

the fluorescence spectra of SiC, SiC/PAA and SiC/Fe<sub>3</sub>O<sub>4</sub> nanoparticles were detected (Fig. 4b). SiC and SiC/PAA nanoparticles had similar fluorescence spectra as well and fluorescence intensity of SiC/PAA nanoparticles was slightly higher than that of SiC. Compared to SiC and SiC/PAA nanoparticles, SiC/Fe<sub>3</sub>O<sub>4</sub> nanoparticles had a lowest fluorescence intensity and peak value was at 275 nm. The fluorescence intensity is in relation to the separation of photo-generated electrons and holes and lower fluorescence intensity indicates effective separation of photo-generated electrons and holes, namely, higher photocatalytic efficiency.<sup>29</sup> The lowest spectra intensity revealed that SiC/Fe<sub>3</sub>O<sub>4</sub> nanoparticles had higher photocatalysis efficiency than SiC and SiC/PAA nanoparticles. The recombination of wide band gap nanoparticles (SiC) and narrower ones (Fe<sub>3</sub>O<sub>4</sub>) may enhance the separation rate of photo-generated electrons and holes and avoid effectively the recombination of electrons and holes so that the absorption ability and photocatalytic efficiency can be improved.<sup>30</sup> And then more electrons can participate in photocatalytic reaction and photo-fermentation process. Finally, total hydrogen yield of combined system was enhanced.

The Raman spectra of nanoparticles were analyzed about the substance composition and structure<sup>31</sup> to reflect the electron transfer behavior.<sup>32</sup> The peaks of SiC nanoparticles centered at 781.8 and 938.6 cm<sup>-1</sup> were characteristic of the transverse optical (TO) mode and longitudinal optical (LO) mode, respectively.<sup>33</sup> The spectra of

SiC/PAA nanoparticles only had a peak located at 777.3 cm<sup>-1</sup> corresponding to TO mode, which indicated that TO mode was slightly shifted to lower wavelength for 4.5 cm<sup>-1</sup> compared with SiC nanoparticles and LO mode disappeared (Fig. 5a). Thus, electron transfer behaviour had taken place between SiC and PAA. The spectra of SiC/Fe<sub>3</sub>O<sub>4</sub> nanoparticles had peaks located at 788.6 and 954.5 cm<sup>-1</sup> shifted to higher wavelength for 6.8 and 15.9 cm<sup>-1</sup> compared with SiC nanoparticles. It was suggested that electron transfer behaviour had taken place between SiC and Fe<sub>3</sub>O<sub>4</sub> from the shift of Raman peaks as well.

The XRD patterns of SiC, SiC/PAA and SiC/Fe<sub>3</sub>O<sub>4</sub> nanoparticles indicating the phase composition were presented in Fig. 5b. SiC nanoparticles displayed diffraction peaks at 35.5°, 41.4°, 60.0°, 71.8° and 75.4° corresponding to the (111), (200), (220), (311) and (222) planes of the crystalline cubic zinc-blended form of 3C-SiC ( $\beta$ -SiC) according to JCPDS Card 75-0254, respectively. After SiC nanoparticles were coated with PAA, diffraction peaks of SiC/PAA nanoparticles at 35.5°, 41.4°, 60.0°, 71.8° and 75.4° did not change, which indicated that the surface modification could only modified surface defects and had no effect on the phase composition of SiC nanoparticles. After SiC nanoparticles were loaded with Fe<sub>3</sub>O<sub>4</sub>, new diffraction peaks of SiC/Fe<sub>3</sub>O<sub>4</sub> nanoparticles appeared at 30.0°, 35.5°, 43.1°, 57.0° and 62.6° corresponding to the (220), (311), (400), (511) and (440)

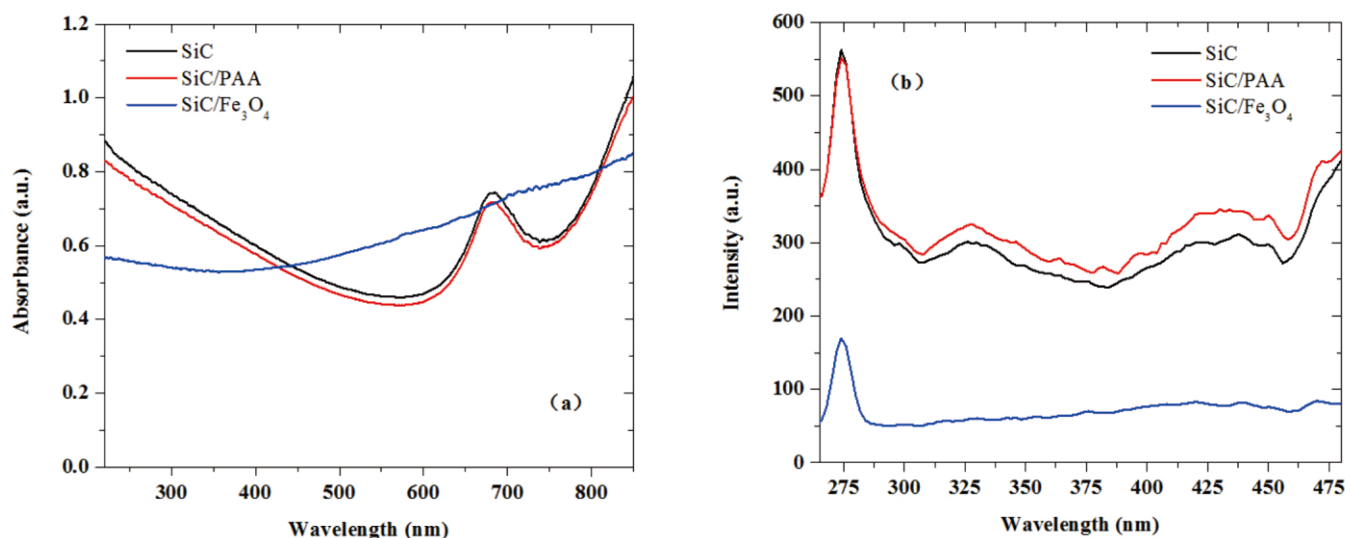


Fig. 4 The ultraviolet-visible absorption spectra (a) and the fluorescence spectra (b) of nanoparticles.

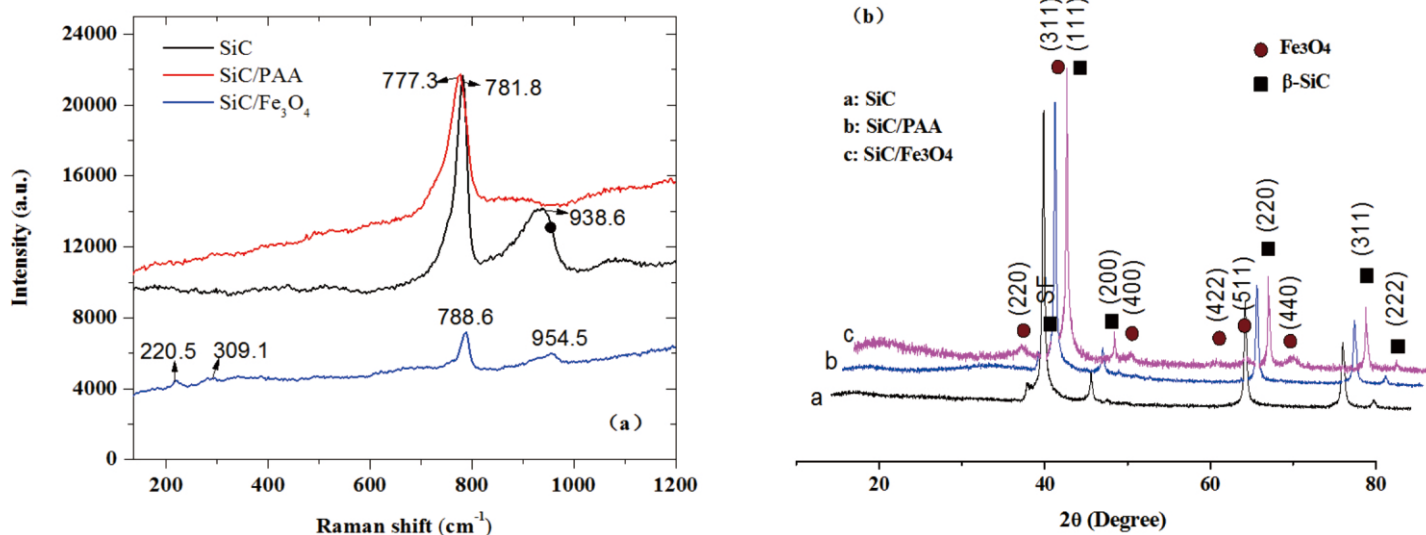


Fig. 5 The Raman spectra (a) and the XRD patterns (b) of nanoparticles.

planes of the cubic spinel crystal structure of Fe<sub>3</sub>O<sub>4</sub> according to JCPDS Card 19-0629, respectively, while diffraction peaks of 3C-SiC (β-SiC) remained the same and any other peak could not be detected. The results showed that SiC/Fe<sub>3</sub>O<sub>4</sub> nanoparticles had achieved a high purity.

The surface elements composition and content of the nanoparticles were analyzed by the XPS patterns in Table S1. Experimental results presented that three nanoparticles contained C, O and Si elements. Beyond that, SiC/Fe<sub>3</sub>O<sub>4</sub> nanoparticles contained Fe element. It was inferred that part of SiC nanoparticles were transformed into SiO<sub>2</sub> caused by the oxidation during the preparation and storage. Remarkably increasing about O element content of SiC/PAA and SiC/Fe<sub>3</sub>O<sub>4</sub> nanoparticles was due to the loading of PAA and Fe<sub>3</sub>O<sub>4</sub>. However, Si element decreased obviously on the contrary. The ratio of C/Si and O/Si of SiC/PAA and SiC/Fe<sub>3</sub>O<sub>4</sub> nanoparticles were higher than SiC, indicating that the two modification methods had effect on the composition and content of surface element to some extent.

The surface carbon-containing functional group contents of the nanoparticles were analyzed by the XPS patterns in Table S2. The results showed that C-C functional group content of SiC/PAA and SiC/Fe<sub>3</sub>O<sub>4</sub> nanoparticles was reduced greatly. However, both C-O and C=O functional group contents of SiC/PAA nanoparticles increased, especially for C=O functional group. In addition, O-C=O functional group content of SiC/Fe<sub>3</sub>O<sub>4</sub> nanoparticles was significantly increased from 0.06% to 14.78% compared to SiC nanoparticles. The surface silicon-containing functional groups contents of the nanoparticles were analyzed by the XPS patterns in Table S2. The results presented that C-Si functional group content of SiC/PAA and SiC/Fe<sub>3</sub>O<sub>4</sub> nanoparticles was reduced, while C-O-Si functional group content increased. The binding energy of two XPS peaks differed by 1.5 eV. A definite proportion of Si element of SiC/PAA and SiC/Fe<sub>3</sub>O<sub>4</sub> nanoparticles increased by 1.5 eV on the binding energy compared with SiC, which was relate to the chemical binding state of element. Binding of PAA and Fe<sub>3</sub>O<sub>4</sub> to SiC produced C-O-Si chemical bonds, making electrons around Si move to O with

higher electronegativity. Consequently, the binding energy of SiC increased after the modification process. The surface ferrum element content of SiC/Fe<sub>3</sub>O<sub>4</sub> nanoparticles was analyzed by the XPS patterns in Table S3. The results indicated that Fe element characteristic peaks of Fe2p<sub>3/2</sub> and Fe2p<sub>1/2</sub> accounted for 43.4% and 25.34%, respectively. Fe<sub>3</sub>O<sub>4</sub> was compounded effectively with SiC nanoparticles. The XPS analysis revealed that two modification methods had influence on the composition and content of surface functional group as well.

The dispersity of nanoparticles in the hydrogen production medium was measured by the zeta potential as shown in Fig. 3d. The zeta potentials of three nanoparticles were below zero during pH of 6-9. SiC/PAA nanoparticles had lower zeta potential than others. It is reported that the dispersity of nanoparticles increased with the absolute value of zeta potential. Results presented that the dispersity of SiC/PAA nanoparticles was enhanced by coating with PAA.

Here a conclusion can be reached SiC/Fe<sub>3</sub>O<sub>4</sub> nanoparticles with excellent photocatalytic ability were synthesized by using semiconductor compound modification. Especially, SiC/Fe<sub>3</sub>O<sub>4</sub> nanoparticles exhibited an ability of hydrogen production from water or medium under visible light irradiation. All above characters of SiC/Fe<sub>3</sub>O<sub>4</sub> nanoparticles implied it can improve photo-fermentative hydrogen production because of its advantages after modification.

### 3.3 The characterizations of photo-fermentative bacteria for enhancing H<sub>2</sub> production

The SEM images of aggregation morphology of strain A7 with different nanoparticles under incandescent were displayed in Fig. 6(a-d). There were obvious differences in bacterial aggregation of strain A7. Bacterial cells presented loose state without any nanoparticles. When the nanoparticles were added in the medium, tight connection was seen among bacterial cells. In addition, the extracellular polymers (EPS) were observed by the addition of nanoparticles, especially for SiC/Fe<sub>3</sub>O<sub>4</sub> nanoparticles.

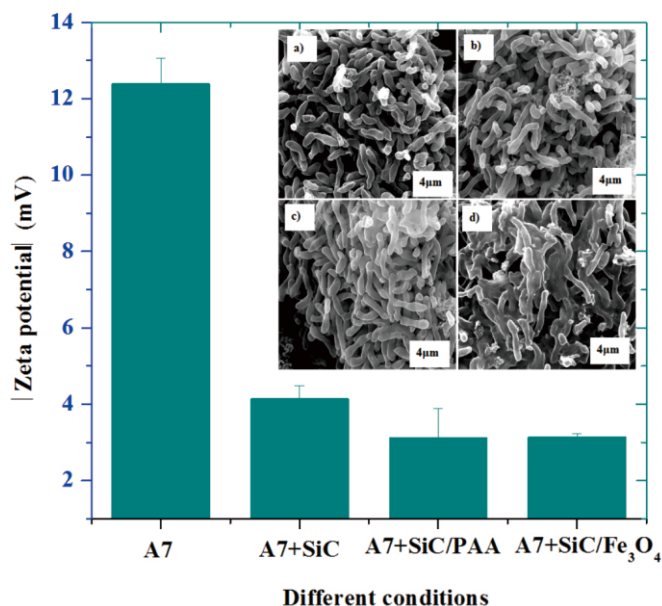


**Fig. 6** The zeta potential of strain A7 with different nanoparticles and the aggregation morphology of strain A7 with different nanoparticles under incandescent lamps. a) Without nanoparticles. b) SiC. c) SiC/PAA. d) SiC/Fe<sub>3</sub>O<sub>4</sub>.

The absolute value of zeta potential of the strain A7 with three nanoparticles in the hydrogen production medium was shown in Fig. 6. Experimental results indicated that the absolute value of zeta potentials of the strain A7 was lower than that of the control obviously and achieved the minimum with SiC/Fe<sub>3</sub>O<sub>4</sub> nanoparticles. It has been reported that the bacterial aggregation performance of microorganism increased with the decrease of absolute value of zeta potential.<sup>40</sup> Consequently, results presented that the bacterial aggregation performance of strain A7 was greatly enhanced by SiC/Fe<sub>3</sub>O<sub>4</sub> nanoparticles. The zeta potential is a key indicator of the degree of electrostatic repulsion between adjacent bacterial cells. Bacterial cells with high absolute  $\zeta$  potential (negative or positive) are electrically stabilized, while cells with low zeta potentials tend to flocculate, which is favorable to photo-hydrogen production.<sup>40</sup>

The surface elements composition and content of strain A7 with different nanoparticles were analyzed by the XPS patterns in Table S4. Experimental results presented that strain A7 contained C, O, N, P, Cl, Na and Si elements. The content of each element was different with the addition of three nanoparticles. The content of C and N was increasing while content of O and Na was decreasing, which indicated that the nanoparticles had influence on the content of surface element of strain A7.

The surface carbon-containing functional groups contents of strain A7 with different nanoparticles were analyzed by the XPS patterns in Table S5. The results showed that C-C functional group content was similar, C-O and C=O functional group contents were increased obviously and O-C=O functional group content was reduced greatly with three nanoparticles. The content of C-O functional group achieved the maximum (16.97%) while O-C=O functional group achieved the minimum (14.08%) with SiC/Fe<sub>3</sub>O<sub>4</sub> nanoparticles. The surface oxygen-containing functional groups contents of strain A7 with different nanoparticles were analyzed by the XPS patterns in Table S5. The results presented that the content of O-C functional group decreased and content of O=C functional group increased with SiC nanoparticles while the results of SiC/PAA and SiC/Fe<sub>3</sub>O<sub>4</sub> nanoparticles were on the contrary. The XPS analysis revealed that the nanoparticles had effect on the composition and content of surface functional group to a great extent. It is reported that surface functional group has great influence on the bacterial aggregation performance of photo-fermentation bacteria and the C-O, C=O and O-C functional groups could improve the bacterial aggregation while the C-C, O-C=O and O=C functional groups were on the contrary.<sup>40</sup> The contents of C-O and C=O increased and O-C=O decreased with three nanoparticles so that the bacterial aggregation performance of strain A7 was enhanced. What's more, the contents of C-O and O-C functional groups were the highest while O-C=O and O=C were the lowest with SiC/Fe<sub>3</sub>O<sub>4</sub> nanoparticles. Consequently, the enhancement of bacterial aggregation performance of strain A7 was optimized with SiC/Fe<sub>3</sub>O<sub>4</sub> nanoparticles.

Nitrogenase and up-take hydrogenase are the key enzymes in photo-fermentative hydrogen production. Nitrogenase has positive influence on hydrogen production while up-take hydrogenase is on the contrary. Therefore, hydrogen production performance of strain A7 strongly depends on the activity of hydrogen production related enzymes, especially nitrogenase.

The nitrogenase activity of strain A7 in the hydrogen production experiments with incandescent lamps were illustrated in Fig. 7a. Nitrogenase activity with nanoparticles is higher than that of the control during entire hydrogen production and increased

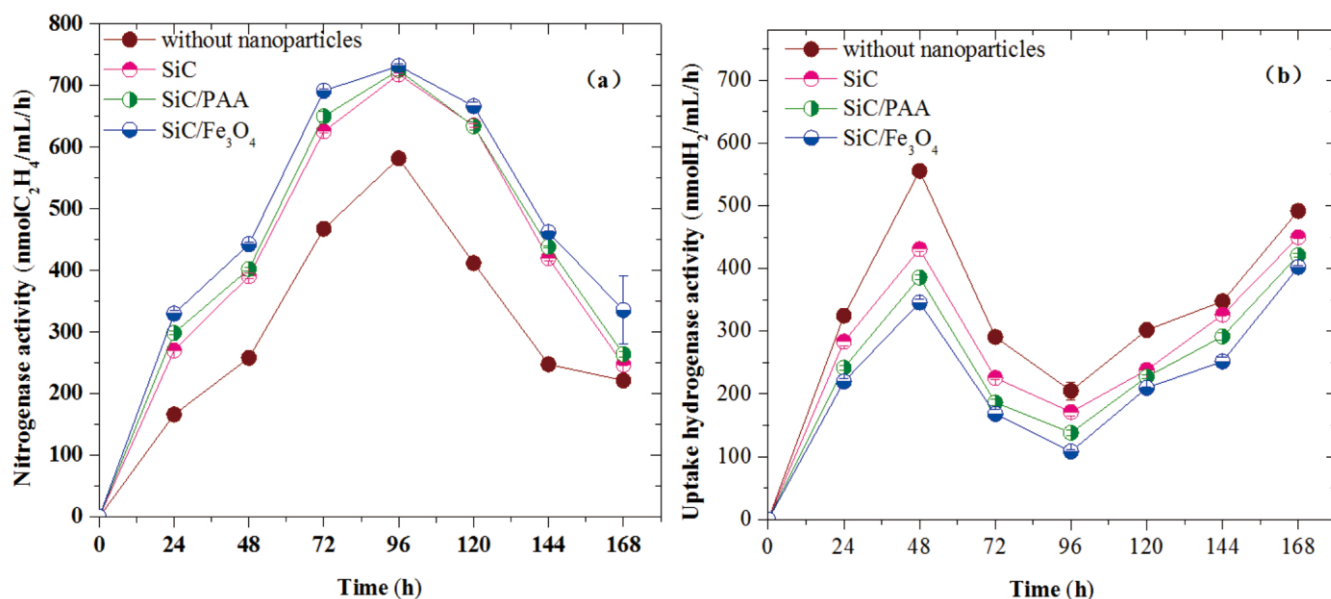


Fig. 7 The effects of nitrogenase and uptake hydrogenase activity of strain A7 with different nanoparticles. (a) nitrogenase activity (b) uptake hydrogenase activity.

gradually at first 4 days and decreased subsequently. The maximum nitrogenase activity achieved 731.8 nmol C<sub>2</sub>H<sub>4</sub>/mL/h in the presence of SiC/Fe<sub>3</sub>O<sub>4</sub> nanoparticles at 4<sup>th</sup> day and was improved by 25.8% compared with the control (581.7 nmol C<sub>2</sub>H<sub>4</sub>/mL/h). It was concluded that nitrogenase activity of strain A7 on hydrogen production was enhanced remarkably with the addition of SiC/Fe<sub>3</sub>O<sub>4</sub> nanoparticles, which is the most direct evidence for enhancing photo-hydrogen production. The uptake hydrogenase activity of strain A7 in the hydrogen production experiments with incandescent lamps were presented in Fig. 7b. Uptake hydrogenase activity increased gradually at first 2 days and decreased at the 3<sup>rd</sup> and 4<sup>th</sup> day then increased again at last 3 days. The maximum uptake hydrogenase activity achieved 555.5 nmol H<sub>2</sub>/mL/h at the 2<sup>nd</sup> day. Experimental results showed that the uptake hydrogenase activity were lower than that of the control obviously and achieved the minimum with SiC/Fe<sub>3</sub>O<sub>4</sub> nanoparticles. It confirmed that uptake hydrogenase activity of strain A7 was inhibited obviously when the SiC/Fe<sub>3</sub>O<sub>4</sub> nanoparticles were used in system and more hydrogen was produced, so hydrogen production was enhanced significantly and hydrogen yield was at a high level.

According to Raman spectra of photosynthetic bacteria there were four characteristic peaks located at 1520, 1160, 1010 and 938.6 cm<sup>-1</sup> corresponding to the stretching modes of C=C bonds ( $\nu_1$  modes), stretching modes of C-C bond mixed with bending modes of C-H bonds ( $\nu_2$  modes), stretching modes of C-CH<sub>3</sub> bonds ( $\nu_3$  modes) and out-of plane C-H bonds modes ( $\nu_4$  modes), respectively.<sup>34,35</sup> In addition, characteristic Raman peaks at approximately 1220, 1290 and 1360 cm<sup>-1</sup> indicated the stretching modes of amide III and deformation vibration modes of CH and CH<sub>2</sub> of protein, respectively.<sup>36</sup> The Raman spectra of strain A7 with different nanoparticles under incandescent lamps were analyzed to reflect the electron transfer behaviour<sup>37,38</sup> as shown in Fig. 8.

On the 1st day, the Raman peaks of strain A7 under incandescent lamps located at 1011, 1159, 1218, 1291, 1370 and 1518 cm<sup>-1</sup>. Raman peaks at 1011, 1159 and 1518 cm<sup>-1</sup> corresponded to characteristic peaks of carotenoid. Raman peaks at 1218, 1291 and

1370 cm<sup>-1</sup> corresponded to characteristic peaks of protein. When the nanoparticles were added in the medium, the Raman peaks were slightly shifted to lower wavelength. The change of Raman peaks was taken place on the 3<sup>rd</sup>, 5<sup>th</sup> and 7<sup>th</sup> day as well. On the 3<sup>rd</sup> day of hydrogen production, almost all peaks were shifted. The addition of nanoparticles changed Raman peaks of strain A7 indicating that the environment in the bacterial cells had changed<sup>39</sup> and electron transfer behaviour had taken place between strain A7 and nanoparticles. It was indicated that the electron was transferred from the SiC/Fe<sub>3</sub>O<sub>4</sub> nanoparticles with high photocatalysis ability to the enzyme system relative with hydrogen production of bacterium strain A7, which is favor to hydrogen production.

#### 4. Discussion

Our work has successfully synthesized SiC/Fe<sub>3</sub>O<sub>4</sub> nanoparticles by semiconductor compound modification and SiC/Fe<sub>3</sub>O<sub>4</sub> nanoparticles exhibiting strong visible light absorption and enhanced photocatalytic activity. Photo-fermentative hydrogen production of *Rhodospseudomonas* sp. nov. strain A7 by the addition of SiC, SiC/PAA and SiC/Fe<sub>3</sub>O<sub>4</sub> nanoparticles with photocatalytic ability was investigated. The results showed that these three nanoparticles promoted photo-fermentative hydrogen production, and hydrogen production could be most significantly enhanced by the addition of 100 mg/L SiC/Fe<sub>3</sub>O<sub>4</sub> nanoparticles with photocatalytic ability. The maximum volume, average content and yield of hydrogen achieved 2474 mL/L-culture, 88.9% and 3.02 mol/mol-acetate, respectively. The volume and yield of hydrogen production by combined system of strain A7 and SiC/Fe<sub>3</sub>O<sub>4</sub> nanoparticles increased about 34.4% and 14%. Importantly, this work first found that photocatalysis of SiC/Fe<sub>3</sub>O<sub>4</sub> nanoparticles and photo-fermentation of photo-fermentative bacteria were realized simultaneously for hydrogen production. The mechanism of enhancement in hydrogen production was studied from following respects: photocatalysis ability of SiC/Fe<sub>3</sub>O<sub>4</sub> nanoparticles, activity of photo-fermentative bacteria and synergy of them. After modification, SiC/Fe<sub>3</sub>O<sub>4</sub> nanoparticles had excellent photocatalysis ability from water or medium to hydrogen

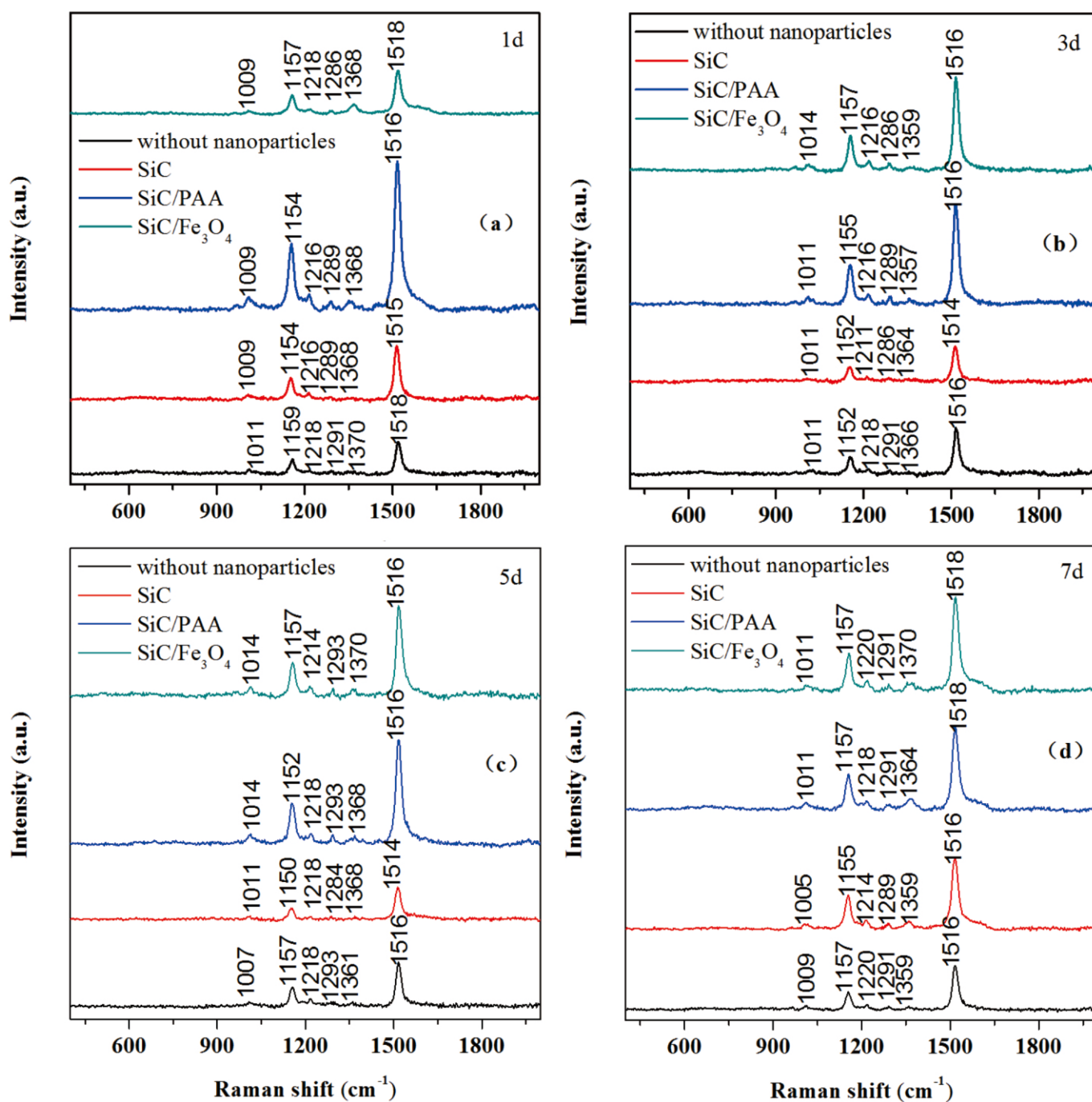


**Fig. 8** The Raman spectra of strain A7 with different nanoparticles under incandescent lamps. a)  $\text{H}_2$  production 1d. b)  $\text{H}_2$  production 3d. c)  $\text{H}_2$  production 5d. d)  $\text{H}_2$  production 7d.

under visible light irradiation. This also was an evidence of enhanced additional hydrogen yield of alone photo-fermentative hydrogen production. In addition, SiC/ $\text{Fe}_3\text{O}_4$  nanoparticles added into photo-fermentative hydrogen production system and it changed the composition and content of surface elements further improved the bacterial aggregation performance. These changes were favorable to enhance hydrogen production by photo-fermentative bacteria.<sup>40</sup> And Si elements were also detected on the surface of photo-fermentative bacterial cell (Table-S4). This result suggested that nanoparticles may present on the cell's surface and promoted photo-generated electron transfer between nanoparticles and

bacterial cell. More importantly, the addition of SiC/ $\text{Fe}_3\text{O}_4$  nanoparticles could obviously promote the activity of nitrogenase and inhibit the activity of uptake hydrogenase in large extent compared with photo-fermentative bacteria without nanoparticles. These two enzymes were key factors determining photo-hydrogen production performance.<sup>11</sup> A study demonstrated that transfer of photo-generated electron can promote the relative enzyme activity of dark-fermentative hydrogen production.<sup>42</sup> Therefore, we propose a combination model for describing hydrogen production process by SiC/ $\text{Fe}_3\text{O}_4$  nanoparticles and photo-fermentation (Fig. 9). During photo-fermentation, the photosynthetic system of photo-fermentative

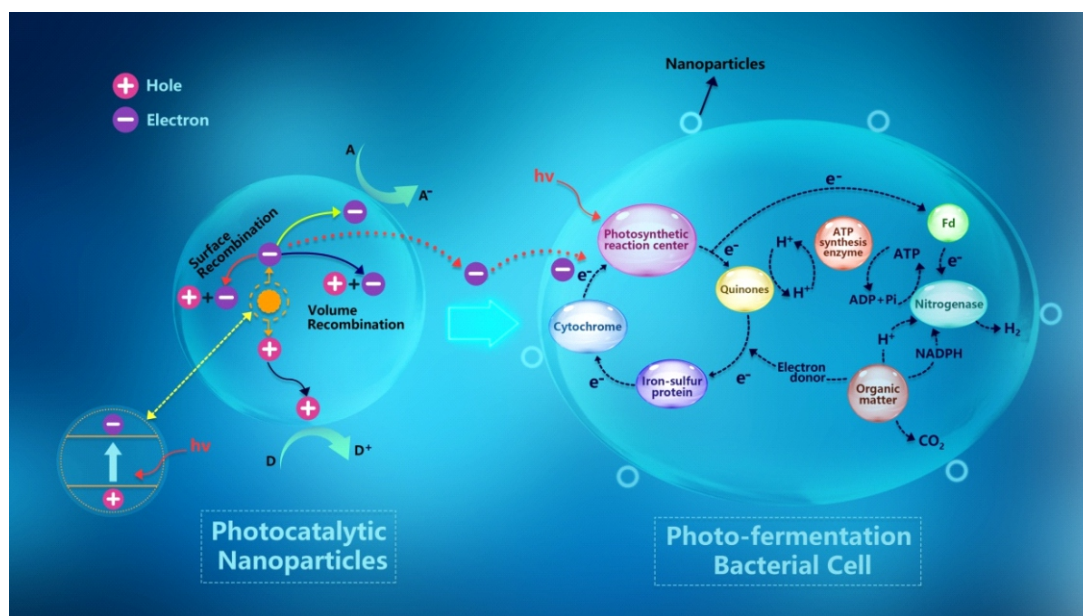


Fig. 9 Schematic diagram for  $H_2$  production by combining nanoparticles with photo-fermentation.

bacteria absorbed light energy to produce high-energy electrons, which could pass through the developmental electron transport chains. The nitrogenase of photo-fermentative bacteria could use ATP that produced by high-energy electrons in the photophosphorylation process and convert protons to hydrogen. In this process, organic matter (short chain organic acids) was as proton donors. So, there are more electrons and protons, and more hydrogen was produced under the catalysis of nitrogenase. During the photoexcitation process of photocatalytic nanoparticles, electrons existing in the valence band (VB) are excited to the conduction band (CB). This is leading to the results of leaving holes in VB and generating photo-electron ( $e^-$ ) and hole ( $h^+$ ) pairs, which can participate in reduction and oxidation reactions, respectively. And then the holes and photo-generated electrons will separate from each other. Some of them will participate in surface recombination or volume recombination. Others will move to different locations on the surface of the nanoparticles to complete reduction and oxidation reactions.

In this work, obtained SiC/Fe<sub>3</sub>O<sub>4</sub> nanoparticles by SiC modification can obviously stop the recombination of the photo-generated electrons and holes. More photo-generated electrons participated in photo-fermentation process. The shift of Raman peaks of strain A7 also demonstrated that produced photo-induced electrons could be transferred across cell membrane into bacterial cell and further transported by electron transport chains to enzyme system of photo-fermentative bacteria for hydrogen production. Combining AgInS<sub>2</sub>/In<sub>2</sub>S<sub>3</sub> and *E. coli* can increase the amount of photo-generated electrons for participating in the biohydrogen production process by preventing the recombination of holes and photo-generated electrons.<sup>41</sup> In addition, excess photo-generated electrons could enhance the amount of electrons for photo-hydrogen production or accelerate the electron transfer rate of electrons to nitrogenase, which was helpful to produce more hydrogen. Thus, the hydrogen production ability, utilization and conversion efficiency of substrate in combined system were improved. This work could provided an efficient avenue for clean energy production technology

dependent on solar energy.

## 5. Conclusions

This work has successfully synthesized SiC/Fe<sub>3</sub>O<sub>4</sub> nanoparticles with strong photocatalytic activity under visible light irradiation. Photo-fermentative hydrogen production could be most significantly enhanced by the addition of 100 mg/L SiC/Fe<sub>3</sub>O<sub>4</sub> nanoparticles. Importantly, photocatalysis and photo-fermentation were realized simultaneously for hydrogen production. The addition of SiC/Fe<sub>3</sub>O<sub>4</sub> nanoparticles could improve the bacterial characters that were favor to hydrogen production. And it could promote the activity of nitrogenase and inhibit the activity of uptake hydrogenase. In addition, photocatalytic nanoparticles could produce photo-generated electrons participated in photo-fermentation process. This was helpful to promote and accelerate the electron transfer rate of the photo-fermentative hydrogen production system. Consequently, the hydrogen production ability was obviously improved.

## Conflict of interest

There are no conflicts to declare.

## Acknowledgements

We are grateful to Financial supports from the National Natural Science Foundation of China (No. 51678186), State Key Laboratory of Urban Water Resource and Environment (Harbin Institute of Technology) (No. 2017DX13) and Postdoctoral Scientific Developmental Fund of Heilong Jiang Province (No. LBH-Q16080)

## References

1. M. Cao, X. Wang, W. Cao, X. Fang, B. Wen, J. Yuan, *Small*, 2018, **14**,1800987.
2. B. Wen, M. Cao, M. Lu, W. Cao, H. Shi, J. Liu, X. Wang, H. Jin, X. Fang, W. Wang, J. Yuan, *Adv. Mater.*, 2014, **26**, 3484-3489.
3. J. Turner, *Science*, 2004, **305**, 972-974.

4. J. Bartels, M. Pate, N. Olson, *Int. J. Hydrogen Energy*, 2010, **35**, 8371-8384.
5. T. Keskin, M. Abo-Hashesh, P. Hallenbeck, *Bioresour. Technol.*, 2011, **102**, 8557-8568.
6. K. Nakata, A. Fujishima, *J. Photochem. Photobiol., C*, 2012, **13**, 169-189.
7. K. Maeda, K. Domen, *J. Phys. Chem. Lett.*, 2010, **1**, 2655-2661.
8. P. Maruthamuthu, S. Muthu, K. Gurunathan, M. Ashokkumar, M. V. C. Sastri, *Int. J. Hydrogen Energy*, 1992, **17**, 863-866.
9. B. Liu, Y. Jin, Z. Wang, D. Xing, C. Ma, J. Ding, N. Ren, *Int. J. Hydrogen Energy*, 2017, **42**, 18279-18287
10. A. Pandey, K. Gupta, A. Pandey, *Biomass Bioenergy*, 2015, **72**, 273-279.
11. Y. Zhao, Y. Chen, *Environ. Sci. Technol.*, 2011, **45**, 8589-8595.
12. V. Nikandrov, M. Shlyk, N. Zorin, I. Gogotov, A. Krasnovsky, *FEBS Lett.*, 1988, **234**, 111-114.
13. K. Gurunathan, *J. Mol. Catal. A: Chem*, 2000, **156**, 59-67.
14. W. Choi, A. Termin, M. R. Hoffmann, *J. Phys. Chem.*, 1994, **98**, 13669-13679.
15. V. Etacheria, C. D. Valentinc, J. Schneiderd, D. Bahnemannd, S. C. Pillai, *J. Photochem Photobiol C*, 2015, **25**, 1-29.
16. L. Zhang, Y. Li, Q. Zhang, H. Wang, *Cryst. Eng. Comm.*, 2013, **15**, 5986-5993.
17. L. Zhang, W. Yu, C. Han, J. Guo, Q. Zhang, H. Xie, Q. Shao, Z. Sun, Z. Guo, *J. Electrochem. Soc.*, 2017, **164**, H651-H656.
18. L. Zhang, Q. Zhang, H. Xie, J. Guo, H. Lyuc, Y. Li, Z. Sun, H. Wang, Z. Guo, *Appl. Catal. B: Environ.*, 2017, **201**, 470-478.
19. M. Wang, J. Chen, X. Liao, Z. Liu, J. Zhang, L. Gao, Y. Li, *Int. J. Hydrogen Energy*, 2014, **39**, 14581-14587.
20. J. Y. Hao, Y. Y. Wang, X. L. Tong, G. Q. Jin, X. Y. Guo, *Int. J. Hydrogen Energy*, 2012, **37**, 15038-15044.
21. X. Liao, J. Chen, M. Wang, Z. Liu, L. Ding, Y. Li, *J. Alloys Compounds*, 2016, **658**, 642-648.
22. B. F. Liu, Y. R. Jin, Q. F. Cui, G. J. Xie, Y. N. Wu, N. Q. Ren, *Int. J. Hydrogen Energy*, 2015, **40**, 8661-8668.
23. H. Zhang, Y. Xu, J. Zhou, J. Jiao, Y. Chen, H. Wang, C. Liu, Z. Jiang, Z. Wang, *J. Mater. Chem. C*, 2015, **3**, 4416-4423.
24. C. Liang, C. Liu, H. Wang, L. Wu, Z. Jiang, Y. Xu, B. Shen, Z. Wang, *J. Mater. Chem. A*, 2014, **2**, 16397-16402.
25. Y. Zhang, R. Burris, P. Ludden, , *J. Bacteriology*, 1995, **177**, 2354-2359.
26. T. Goodman, P. Hoffman, *J. Clin. Microbiol.*, 1983, **18**, 825-829.
27. J. Hao, Y. Wang, X. Tong, G. Jin, X. Guo, *Int. J. Hydrogen Energy*, 2012, **37**, 15038-15044.
28. Y. Li, X. Cheng, X. Ruan, H. Song, Z. Lou, Z. Ye, L. Zhu, *Nano Energy*, 2015, **12**, 775-784.
29. E. Su, B. Huang, C. Liu, M.Y. Wey, *Renew Energy*, 2015, **75**, 266-271.
30. A. J. Cowan, J.R. Durrant, *Chem. Soc. Rev.*, 2013, **42**, 2281-2293.
31. C. Fang, R. Frontiera, R. Tran, R. Mathies, *Nature*, 2009, **462**, 200-204.
32. P. Kukura, D. McCamant, S. Yoon, , *Science*, 2005, **310**, 1006-1009.
33. M. Bechelany, A. Brioude, D. Cornu, G. Ferro, P. Miele, *Adv. Funct. Mater.*, 2007, **17**, 939-943.
34. A. Gall, A. Gardiner, R. Cogdell, B. Rober, *FEBS Lett.*, 2006, **580**, 3841-3844.
35. B. Robert, *Photosynth Res.*, 2009, **101**, 147-155.
36. W. E. Huang, M. J. Bailey, I. P. Thompson, A. S. , A. J. , *Microb Ecol.*, 2007, **53**, 414-425.
37. S. Han, Y. Ching, D. Rousseau, *Nature*, 1990, **348**, 89-90.
38. W. Eisfeld, C. Pusch, R. Diller, R. Lohrmann , M. Stockburger, *Biophys Chem.*, 1993, **32**, 7196-7215.
39. U. Schmid, P. Rösch, M. Krause, M. Harz, J. Popp, K. Baumann, *Chemom. Intell. Lab. Syst.*, 2009, **96**, 159-171.
40. G. Xie, B. Liu, D. Xing, J. Nan, J. Ding, N. Ren, *Biotechnol Biofuels*, 2013, **6**, 64.
41. Z. F. Jiang, B. Wang, J. C. Yu, J. F. Wang, T. C. An, H. J. Zhao, H. M. Li, S.Q. Yuan, P.K. Wong, *Nano Energy*, 2018, **46**, 234-240.
42. K. Sakimoto, A. Wong, P. Yang, *Science*, 2016, **351**, 74-77.